Comparison of the linking arm effect on the biological performance of a CD31 agonist directly grafted on L605 CoCr alloy by a plasma-based multistep strategy

Sergio Diaz-Rodriguez,[1] Caroline Loy,[1] Pascale Chevallier,[1] Céline Noël,[2] Giuseppina Caligiuri,[3,4] Laurent Houssiau,[2] and Diego Mantovani[1,a)]
[1]*Laboratory for Biomaterials and Bioengineering (CRC-I), Department of Min-Met-Mat Engineering and the CHU de Québec Research Center, Laval University, PLT-1745G, Québec G1V 0A6, Canada*
[2]*Laboratoire Interdisciplinaire de Spectroscopie Electronique, Namur Institute of Structured Matter, University of Namur, 61 Rue de Bruxelles, 5000 Namur, Belgium*
[3]*Laboratory for Vascular Translational Science, Institut National de la Santé et de la Recherche Médicale U1148, DHU (Département Hospitalo-Universitaire) FIRE (Fibrosis, Inflammation, REmodelling), Faculty of Medicine Paris-Diderot, University Paris Diderot, Sorbonne Paris Cité, F 75018 Paris, France*
[4]*AP-HP (Assistance Publique-Hôpitaux de Paris), Department of Cardiology and Physiology, University Hospital Xavier Bichat, F 75018 Paris, France*

(Received 22 July 2019; accepted 24 September 2019; published 1 November 2019)

Stents are cardiovascular implants deployed on atherosclerotic arteries that aid in reopening, sustaining, and avoiding their collapse. Nevertheless, postimplantation complications exist, and the risk of the renewal of the plaque subsists. Therefore, enhanced properties are mandatory requirements for clinics. For that purpose, a novel approach allowing the direct-grafting of bioactive molecules on cobalt-chromium devices (L605) has been developed. This original strategy involves the direct plasma functionalization of metallic surfaces with primary amines ($-NH_2$). These groups act as anchor points to covalently graft biomolecules of interest, herein a peptide derived from CD31 (P23) with proendothelialization and antithrombotic properties. However, the biological activity of the grafted peptide could be impacted by its conformation. For this study, glutaric anhydride (GA), a short chain spacer, and polyethylene glycol (PEG) with antifouling properties were used as linking arms (LAs). The covalent grafting of the CD31 agonist on L605 by different LAs (GA-P23 and PEG-P23) was confirmed by XPS and ToF-SIMS analyses. The biological performance of these functionalized surfaces showed that, compared to the electropolished (EP) alloy, grafting the P23 with both LA increases adhesion and proliferation of endothelial cells (ECs) since day 1: EP = 68 ± 10%, GA-P23 = 101 ± 7%, and PEG-P23 = 106 ± 5% of cell viability. Moreover, ECs formed a complete monolayer at the surface, preventing clot formation (hemoglobin-free >80%). The potential of this plasma-based strategy for cardiovascular applications was confirmed by promoting a fast re-endothelialization, by improving the hemocompatibility of the alloy when coupled with the CD31 agonist and by its transfer onto commercial L605 stents, as confirmed by ToF-SIMS. *Published by the AVS.* https://doi.org/10.1116/1.5120902

I. INTRODUCTION

Bare metal stents (BMS) are used to treat chirurgically atherosclerosis, a cardiovascular disease that narrows the artery by the formation of a plaque. These devices are implanted with a balloon catheter that is expanded on the obstructed area, pushing the plaque onto the arterial walls and deploying the device.[1] Nevertheless, complications after implantation exist and in-stent restenosis (ISR), the reformation of the plaque on the stent, might occur.[2,3] These complications can be related to the damage on the endothelium while deploying the device, the overproliferation of smooth muscle cells (SMCs), and thrombus formation.[4] In order to lower complications, one strategy was to load the surface of cardiovascular stents with antiproliferative drugs to avoid the undesired over proliferation leading to the development of drug-eluting stents (DESs).[5] The mechanism of action of the drugs loaded on DES focuses on the inhibition of SMCs proliferation, associated with ISR formation; nevertheless, these drugs also inhibit the proliferation of endothelial cells (ECs), compromising the healing of the endothelium leading to long term complications.[6] Thus, one of the main problems for DES is late ISR, which seems to have shifted the time course of restenosis, from 6–8 months in BMS to >3 years.[7,8] This led to more than 200 000 number of patients developing restenosis each year only in the USA.[9]

In recent years, the research for other bioactive molecules with properties such as antithrombotic, anti-inflammatory, and proendothelialization that can be used to enhance the biological properties of BMS has been performed.[10–13] A short peptide (P23) derived from the platelet endothelial cell adhesion molecule-1 (PECAM-1), also known as cluster of differentiation 31 (CD31), has shown promising results.[14] This protein is present on the surface of platelets, leucocytes, and on the lateral junctions of endothelial cells. It promotes

Note: This paper is part of the Conference Collection on ISSIB 2019: Surface and Interface for Biomaterials.

a)Electronic mail: diego.mantovani@gmn.ulaval.ca

the adhesion and proliferation of endothelial cells while avoiding the activation of platelets, conferring properties desired for the stent application.[15,16]

The immobilization of this short peptide onto metallic surfaces can improve the integration of the cardiovascular device. Common strategies to perform this covalent grafting include the deposition of a polymeric coating that allows the further grafting of the molecule.[17,18] Nevertheless, wet-based deposition techniques do not assure the mechanical stability of this polymeric layer.[19] Another approach to immobilize bioactive molecules onto BMS is the use of plasma polymer coatings. However, the main challenges these coatings face are related to their chemical stability: Potential bond degradation when exposed to the biological medium, leading to coating delamination, and the loss of reactive moieties due to cross-linking reactions inside the plasma reactor, leading to additional functionalization steps before the immobilization of the bioactive molecule.[20] Therefore, a novel multistep strategy to directly functionalize cobalt-chromium alloys with amine groups that can be used as anchor points to graft molecules without the use of any polymeric coating has been developed.[21] These amine groups allow the use of different spacers [linking arms (LAs)] to confer additional properties or to assure the biological activity of the grafted molecule.[22] Furthermore, by avoiding the use of polymeric layers onto the metallic devices, patients with hypersensitivity allergic reactions could potentially use these bioactive stents.[23]

For this study, two different linking arms have been chosen in order to observe the impact of their structure on the biological activity of the peptide: Glutaric anhydride (GA), as a short chain linking arm,[10,22–25] and polyethylene glycol (PEG), as a long chain linking arm known for its antifouling properties.[3,26–28] The characterization of these functionalized surfaces represents a challenge due to its nanometric range, and the use of high-resolution techniques is necessary. The combination of techniques such as XPS and ToF-SIMS allow one to obtain information regarding the chemical composition of the surface, the distribution and conformation of the peptide, which can be further correlated to the biological performance, in terms of endothelialization and hemocompatibility, of the functionalized surface. Moreover, the feasibility of transferring the functionalization from flat samples to cardiovascular devices is also studied by ToF-SIMS imaging.

II. MATERIALS AND METHODS

A. Materials

L605 alloy sheets (wt. %: Co 51%, Cr 20%, W 15%, Ni 10%, Fe $\leq$ 3%, C $\leq$ 0.15%) were purchased from Rolled Alloys Inc. (QC, Canada). ACS grade acetone and methanol were purchased from Fisher Scientific. The following reagents were purchased from Sigma-Aldrich: GA (95%), MES [2-(*N*-morpholino)ethanesulfonic acid, $\geq$99%], and EDAC [1-ethyl-3-(3-dimethylaminopropyl) carbodiimide hydrochloride, $\geq$98%]. Phosphate buffered solution (PBS, 1× powder) and poly(ethylene glycol) bis(carboxymethyl) ether (PEG, average Mn 600) were purchased from Fisher Scientific. Stents were manufactured by Abbott Vascular, model Multi-Link 8 Coronary Stent. The custom 23 amino acids peptide (~10.9 nm length), P23, containing lysine, proline, valine, leucine, and isoleucine in its structure was purchased from Mimotopes (Minnesota, USA).

B. Sample preparation

1. Surface preparation

Round specimens of 13 mm diameter were punched from L605 sheets and cleaned in three successive ultrasonic baths of acetone, water, and methanol for 10 min each. After cleaning, surfaces were electropolished (EP) as previously described.[21] Briefly, the process consists of three successive electropolishing in an acid solution in order to remove the native oxide layer and create a nanosmooth mirrorlike surface with an oxide layer rich in chromium oxides. After electropolishing, samples were exposed to three ultrasonic baths: nanopure water, NaOH 2 N, and nanopure water, to remove any remnants of the electropolishing procedure. The use of EP surfaces as base surface preparation was motivated by bare metal stents which undergo this surface processing after laser cutting during their fabrication.

2. Plasma amination

After sample preparation, the direct plasma functionalization was carried out in an MW plasma reactor fed with nitrogen and hydrogen in a two-step process as described elsewhere.[21] Briefly, plasma amination was performed using a mixture of N_2 and H_2 as feeding gases for the first plasma step, at 150 W during 10 min at 100 mTorr, 5/5 sccm of N_2/H_2, while the second step was performed at 150 W during 30 s at 300 mTorr, 10 sccm of H_2. Reactive amine groups obtained during this functionalization step were used as anchor points for the further grafting of the linking arms.

3. Linking arm grafting

L605 plasma treated disks were submerged in acetone and 0.3 g ml^{-1} of GA was added three times at 0, 20, and 40 min. For PEG, samples were immersed in 0.1 g ml^{-1} PEG solution, pH 4.75 in MES buffer, activated with 3 mg ml^{-1} EDAC added three times at 0, 10, and 20 min. The reaction was completed after 1 h for both linking arms. Once the reaction was finished, samples were vortex washed three times with acetone or MES, for GA and PEG, respectively, five times with de-ionized water, dried, and stored under vacuum before use.

4. Peptide grafting

After the grafting of both linking arms, the activation of their respective terminal carboxylic group (-COOH) was performed in order to further graft the peptide. This activation was performed in 5 ml of MES buffer with 3 mg ml^{-1} EDAC added three times at 0, 10, and 20 min. After 30 min of activation, samples were removed from the tubes to immediately

react with 500 μl of a 2.5×10^{-5}M peptide solution in PBS for 3 h. Once the reaction was finished, samples were vortex washed five times with de-ionized water, dried, and stored under vacuum before further characterization and tests were performed. The complete reaction scheme is shown in Fig. 1. Peptide grafted by glutaric anhydride is labeled as GA-P23 and PEG-P23 for the peptide grafted by PEG.

C. Biological test on flat samples

1. Cell culture and cytotoxicity assays

Human umbilical vein ECs (HUVECs) were isolated as previously described[29] from human umbilical cord samples, obtained from normal term pregnancies. Written informed consent was obtained from all mother donors according to the Declaration of Helsinki. All experiments were performed in compliance with the Canadian Tri-Council Policy Statement: Ethical Conduct for Research Involving Humans and institutional CHU de Quebec—Laval University guidelines. The protocol was approved by the Ethics Committee of the CHU de Quebec Research Centre (CER No. S11-03-168).

HUVECs were cultured in M199 (Life Technologies, 11995-065) supplemented with 1% PenStrep (G1146 Sigma), 5% fetal bovine serum (Life Technologies, 12483-020), 2 ng/ml fibroblast growth factor (0.1%), 1 ng/ml epidermal growth factor (0.2%), 1 μg/ml ascorbic acid (0.1%), 1 μg/ml hydrocortison (0.1%), and 90 μg/ml heparin (1%).

Direct cytocompatibility tests were performed to evaluate cell adhesion and growth over samples. Samples were placed in 24-well plates and sterilized with 70% EtOH for 20 min. Then, a two-well culture-Insert (ibidi) was transferred onto samples. Cells were seeded at a density of 5×10^4 cells/cm^2 in each culture-Insert well. After 24 h, inserts were carefully removed. Cell viability was evaluated 1, 3, and 7 days after seeding, by the AlamarBlue assay (Life Technologies, Burlington, ON, Canada), according to the manufacturer's guidelines. Briefly, the culture medium was replaced with 400 μl of culture medium containing the resazurin dye. After 5 h incubation in standard culture conditions, the fluorescence of the medium was read (kex:560 nm; kem:590 nm). Viability was evaluated considering the fluorescence of the control cells as 100%.

2. Hemocompatibility assays

The coagulation of whole blood in contact with the surfaces of the developed models was evaluated using the hemoglobin-free method. Briefly, 30 μl of human citrated blood were mixed with 6 μl of $CaCl_2$. 0.1M (Sigma) were deposited onto the surfaces of the different samples and incubated thereafter at 37 °C for 10, 20, and 60 min. Directly after, 2 ml of distilled water were added to each sample. The free hemoglobin molecules released in water following hemolysis were measured by reading the absorbance at a 540 nm wavelength by means of a SpectraMax i3x Multi-Mode Plate Reader (Molecular Devices, San Jose, CA, USA). Data were normalized toward the Max Hemoglobin value corresponding to the value obtained by immediate hemolysis after the citrate inhibition by $CaCl_2$. The experiments were performed in triplicate using blood from three different donors.

D. Transfer to cardiovascular devices

Stent functionalization and grafting: The feasibility of transferring the developed multistep plasma procedure for the direct covalent grafting of molecules onto commercial stents has been studied. This was performed using the previously proposed strategy[21] with the following parameters: Plasma amination of the substrates was performed in the after-glow region (7 cm) of MW plasma (Plasmionique Inc., Varennes, Québec, Canada) by means of a two-step process using a mixture of N_2 and H_2 (grades 4.8 and 5.0, respectively, Linde, Québec, Canada) as the feeding gases. The first stage was carried out at 150 W during 10 min at 100 mTorr, 10/10 sccm of N_2/H_2, while the second was

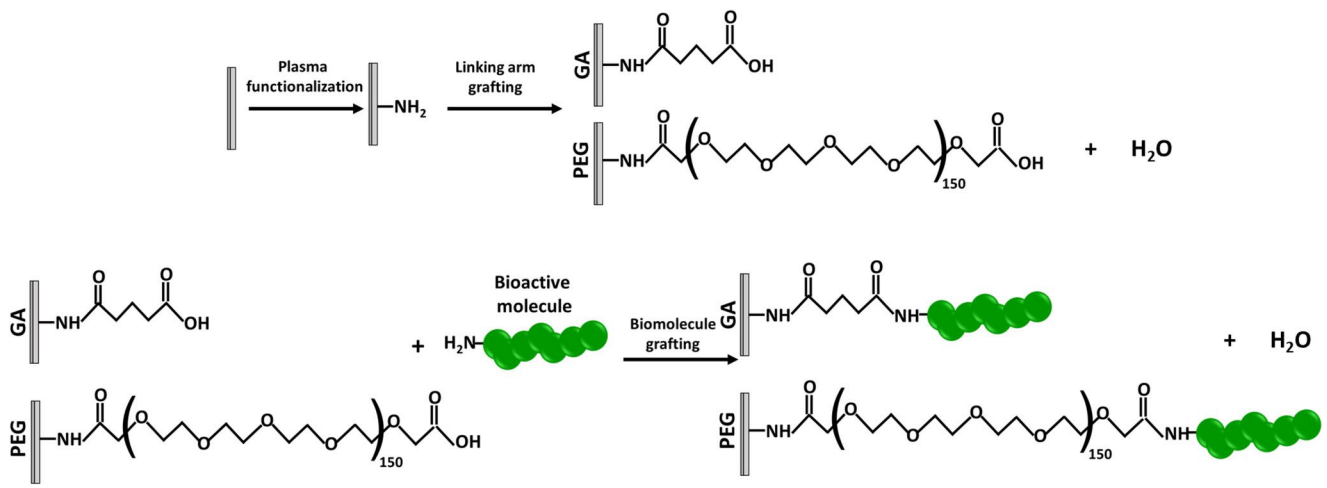

FIG. 1. Reaction scheme of the surface modification of the cobalt-chromium alloy, involving the plasma functionalization to create reactive amine groups used as anchor points for the linking arm grafting, followed by the biomolecule grafting.

performed at 150 W during 30 s at 300 mTorr, 20 sccm of H_2. This plasma amination of stents was performed twice on the device, flipping the stent after the first treatment to create a homogeneous functionalization.

After plasma amination, the grafting of PEG as linking arms and the grafting of the peptide onto the cardiovascular device were performed as previously detailed for flat specimens.

E. Characterization techniques

1. X-ray photoelectric spectroscopy (XPS)

The chemical composition of different surfaces was assessed by XPS (XPS−PHI 5600-ci Spectrometer, Physical Electronics, USA), at a pressure under 10^{-8} Torr, survey analyses were performed with an achromatic Al X-ray source while high-resolution spectra of C1s were obtained using an achromatic Mg X-ray source. The detection was performed at 45° with respect to the surface normal and the analyzed area was 0.05 mm^2 with a depth sensitivity of 5 nm. The spectrometer work function was adjusted to give 285.0 eV for the main C1s peak.

2. Atomic force microscopy (AFM)

Surface texture investigations were performed using the tapping mode on a DimensionsTM 3100 Atomic Force Microscope (Digital Instruments/Veeco) with an etched silicon tip (model NCHV, tip radius = 10 nm, Bruker). Representative areas of $2 \times 2\,\mu m^2$ were recorded and analyzed using the NANOSCOPE ANALYSIS software (Bruker). The root mean square roughness (Rq) was recorded for all surfaces. The measurements were performed in three different areas on three different samples.

3. Immunofluorescence staining

After 1, 3, or 7 days of culture, samples were washed twice with PBS, fixed with 3.7% formaldehyde (Sigma) for 20 min, and treated with 0.5% Triton X-100 in PBS for 30 min at room temperature to permeabilize the cells. The constructs were incubated thereafter for 1 h at room temperature with mouse monoclonal antibody against VE-cadherin (Abcam, Ab7047, dilution 1/50), washed twice with 0.05% Tween 20 in PBS, and finally incubated at room temperature for 1 h with antimouse Alexa Fluor 488 antibody (Life Technologies). Rhodamine-phalloidin (Sigma) and 4′,6-diamidino-2-phenylindole were used to stain the F-actin and nuclei, respectively. Images were obtained under an Olympus BX51 fluorescence microscope.

4. Time of flight-secondary ions mass spectrometry

All ToF-SIMS analyses were performed using a ToF-SIMS IV spectrometer (ION-TOF GmbH, Münster Germany) with the following operating conditions: a pulsed 25 keV Bi_3^+ ion beam (current = 0.37 pA; pulse width = 20 ns; pulse width after bunching = 0.75 ns; repetition rate = 10 kHz) was rastered for an acquisition time of 120 s over areas of $(250 \times 250)\,\mu m^2$ for flat specimens, $(150 \times 150)\,\mu m^2$ and $(500 \times 500)\,\mu m^2$ for stents with a depth sensitivity of <1 nm. The total ion fluence was kept under 10^{12} ions per cm^2 in order to guarantee static conditions. In the meantime, a low-energy electron flood gun was used to ensure charge compensation. The secondary ions were extracted at a 2 kV acceleration voltage. By measuring the time of flight between the sample and the detector and after an appropriate calibration, one has access to the secondary ion mass distribution. In this case, positive and negative spectra were calibrated with the $Cr_2O_2^+$, $C_2H_6N^+$, and $C_4H_8N^+$ peaks and CN^-, CrO_2^-, and I^- peaks, respectively. ToF-SIMS spectra were obtained from 0 to 880 m/z. Fragments of interest for this study are shown in Table I. Briefly, two kinds of fragments were studied: (a) fragments related to the peptide composition[30,31] and (b) fragments related to the surface and the linking arm.[21,32]

5. Statistical analysis

Statistical analysis was carried out using GRAPHPAD 6 (GraphPad Software, La Jolla, CA, USA). Comparisons among groups were performed by unpaired t-test or one-way ANOVA with *post hoc* Tukey test for multiple comparisons. Significance was retained when $p < 0.01$. Data are expressed as mean ± standard deviation ($n = 9$).

III. RESULTS

A. Surface characterization

Changes in the chemical composition of the surface after each grafting step was followed by XPS survey analyses (Table II). A general trend was observed on both GA and PEG when compared to the aminated surface (NH_2): The percentage of nitrogen and metals decreased after the grafting of the linking arm—In the case of nitrogen from 11.0 ± 0.1% on the aminated surface to 5.9 ± 0.5% and 5.1 ± 0.2% for GA and PEG, respectively. The atomic contribution from chromium for the aminated surface and GA was similar, 9.2 ± 0.8% and 9.1 ± 0.6%, respectively, while for PEG was 8.6 ± 0.1%. As regards the percentage of cobalt, a decrease

TABLE I. ToF-SIMS fragments of interest, in positive mode, for the study of the conformation of the peptide. On top, single-letter code of the amino acids and bellow ToF-SIMS fragments for the linking arm (GA and PEG) and for the oxide layer (Chromium oxide) with their respective m/z.

Letter	Amino acid	ToF-SIMS fragment	m/z
V	Valine	$C_4H_{10}N^+$	72.082
P	Proline	$C_4H_8N^+$	70.069
K	Lysine	$C_5H_{10}N^+$	84.083
I	Isoleucine	$C_5H_{12}N^+$	86.097
L	Leucine	$C_5H_{12}N^+$	86.097
	Fragment	ToF-SIMS fragment	m/z
	GA/PEG	$C_2H_5O^+$	45.032
	Oxide layer	$Cr_2O_2^+$	135.871

TABLE II. Surface chemical composition of the L605 after each modification step, assessed by XPS survey analyses. Expressed as the mean ± standard deviation. Analyses performed on three different samples with three points per samples (n = 9). Furthermore, the theoretical composition of the peptide is shown.

Surface	%C	%O	%N	%Cr	%Co
L605 EP	42.9 ± 1.6	46.4 ± 1.1	—	4.8 ± 0.2	—
NH_2	27.5 ± 1.8	49.9 ± 0.8	11.0 ± 0.1	9.2 ± 0.8	2.6 ± 0.2
GA	31.1 ± 1.3	46.5 ± 1.5	5.9 ± 0.5	9.1 ± 0.6	2.0 ± 0.2
GA-P23	39.5 ± 1.2	39.3 ± 0.5	8.3 ± 0.1	7.0 ± 0.4	1.3 ± 0.1
PEG	34.7 ± 1.3	44.3 ± 0.6	5.1 ± 0.2	8.6 ± 0.1	1.8 ± 0.5
PEG-P23	36.4 ± 2.1	42.6 ± 0.7	6.1 ± 0.7	8.3 ± 1.2	1.9 ± 0.5
P23 theoretical	64.7	15.8	19.6	—	—

was observed for both linking arms: from 2.6 ± 0.2% in the NH_2 surface to 2.0 ± 0.2% and 1.8 ± 0.5% for GA and PEG, respectively. Furthermore, the percentage of C increased on LA grafted surfaces when compared to NH_2 surfaces as the LA molecules are rich in carbon, and this increase is more pronounced for PEG than for GA, as expected. Although the LA also contain O, a slight decrease of the O percentage was observed, due to the coverage of the O-rich metal oxide by the LA chains. The peptide grafting efficiency on the LA surfaces was associated with the changes in the nitrogen percentage with a significant increase on the case of glutaric anhydride: From 5.9 ± 0.5% in GA to 8.3 ± 0.1% in GA-P23. In the case of polyethylene glycol as LA, the contribution of nitrogen from the peptide was not as significant as observed on the other LA: From 5.1 ± 0.2% in PEG to 6.1 ± 0.7% for PEG-P23. Furthermore, the percentage of metals continued to decrease with the peptide grafting. Moreover, the percentage of carbon on the surface increased with the grafting of the peptide, as expected due to peptide chemical compositions. The C and N increase was higher for GA-P23 than PEG-P23, suggesting a more efficient grafting on GA than on PEG.

Regarding changes on the roughness of the surface (Fig. 2), a significant increase was noticed after the peptide grafting with both linking arms compared to the aminated sample: from 1.3 ± 0.1 to 1.9 ± 0.2 and 2.5 ± 0.4 nm for GA-P23 and PEG-P23, respectively. Also, the fact that PEG-P23 surface presented a higher Rq than GA-P23 one could be associated with the longer chain in PEG than the one in GA.

B. Biological performance

Two important properties for cardiovascular devices were studied: (1) interaction with endothelial cells by viability, proliferation, and migration tests and (2) hemocompatibility, with a hemoglobin-free test. Endothelial cell viability and proliferation were evaluated by direct seeding HUVECs on different surfaces. As evidenced in Fig. 3, after 24 h the cell viability of the surfaces with the immobilized peptide was higher compared to EP: 68 ± 10% vs GA-P23: 101 ± 7% and PEG-P23: 106 ± 5 ($p < 0.01$). After 3 days, HUVEC viability was still higher on the functionalized surface than EP. Finally, after 7 days, only the PEG-P23 surface showed a significant difference on cell viability to the EP surface: 243% ± 12 vs 216 ± 10%, respectively ($p < 0.01$).

After viability assays, endothelial cell proliferation and migration were studied up to seven days. HUVECs were seeded into a two-well culture-insert which was removed after cell attachment. After the removal, at day 1, a cell-free gap was created in which the cell proliferation can be visualized as the time passed by, to simulate the re-endothelialization process. As observed in Fig. 4, none of the surfaces presented any difference on the first day of the test. After 3 and 7 days, cells started to proliferate on the surfaces of each sample until the gap was filled. At day 3, more ECs are detected in the gap for the PEG-P23 surface compared to the GA-P23 and the EP surfaces, meaning that the migration of the cells appeared to be faster on PEG-P23. At day 7, the gap was completely filled by ECs on the P23 modified surfaces, with both PEG and GA. However, at this time, PEG-P23 showed a higher intensity on the coloration related to the cell junctions (green). This was due to a higher presence of endothelial cells with the best coverage compared to the other surfaces; thus, a complete monolayer was obtained on PEG-P23.

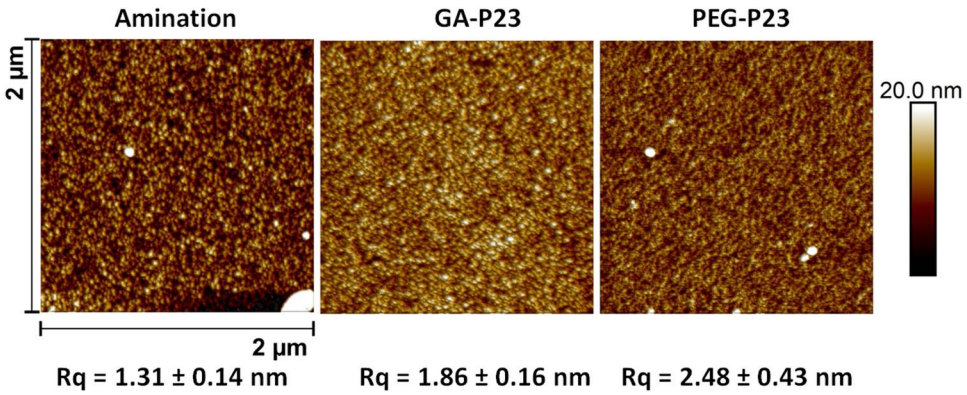

FIG. 2. AFM images $2 \times 2\,\mu m^2$ of the L605 surface after the grafting of the peptide: (a) Amination sample, (b) GA-P23, and (c) PEG-P23. After the grafting of the peptide, there was a significant increase on the surface roughness compared to the plasma aminated L605 surface.

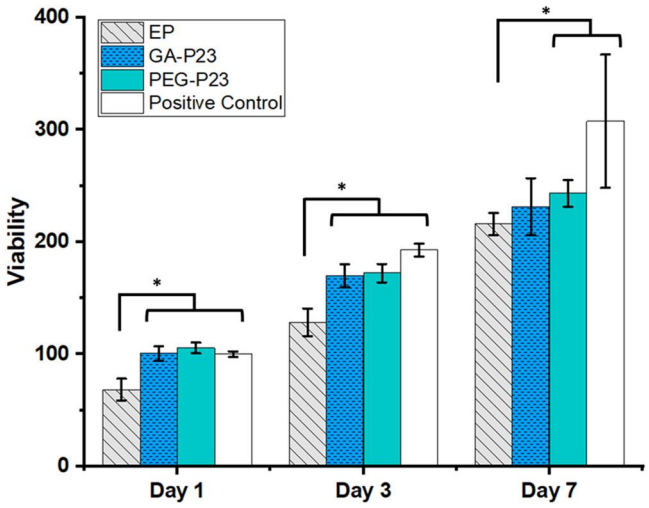

FIG. 3. Endothelial cell viability up to seven days. It was found that grafting the peptide significantly increases the cell viability when compared to the electropolished surface. Only PEG-P23 presents a significant difference to EP on day 7. Samples normalized to control (well plate). Number of samples = 9, $p < 0.01$.

Regarding the hemocompatibility of the surfaces, it was found that surfaces with the P23 peptide can slightly slow down the coagulation rate when compared to the EP surface during the first minutes of the coagulation cascade. As observed in Fig. 5(a), there was a significant difference after 10 min of contact on PEG-P23 and GA-P23 with EP ($p < 0.01$). Following the coagulation kinetics, after 20 min of incubation, there were no significant differences between surfaces and at 30 min blood is completely coagulated (% of free hemoglobin <20%). Furthermore, the blood coagulation was also evaluated on endothelialized surfaces. The selected time point for this experiment was 20 min. This time was chosen according to the previous experiment were blood was nearly coagulated at the surface. The percentage of free hemoglobin for these endothelialized surfaces prevented the formation of blood clots, since it was superior to 80%, as observed in Fig. 5(b). However, no difference was found between EP, GA-P23, and PEG-P23 probably because HUVECs can adhere and also proliferate on the EP surface as shown in Figs. 3 and 4.

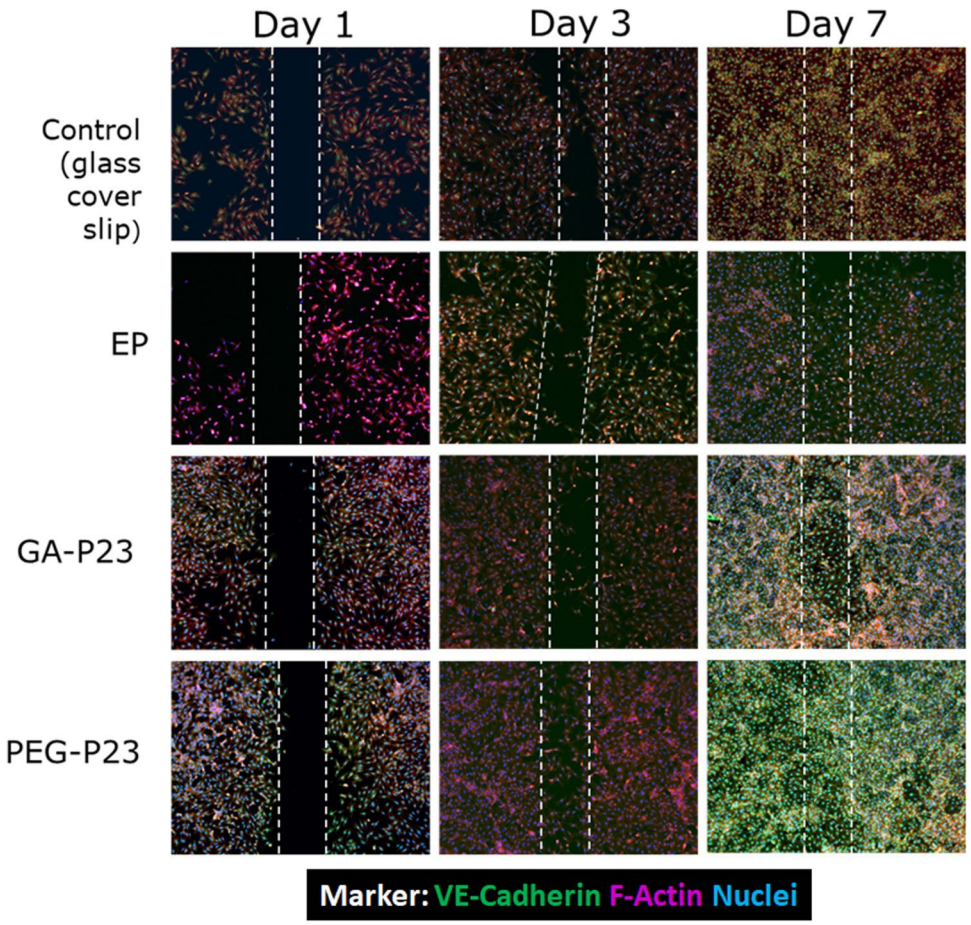

FIG. 4. Endothelial cell migration assay up to seven days. It was found that grafting the peptide by any linking arm increases cell migration up to 7 days. Furthermore, PEG-P23 was the best surface by promoting a complete monolayer and with a demonstrating a higher endothelial cells junction integrity by its intense VE-Cadherin staining after this period compared to the other surfaces.

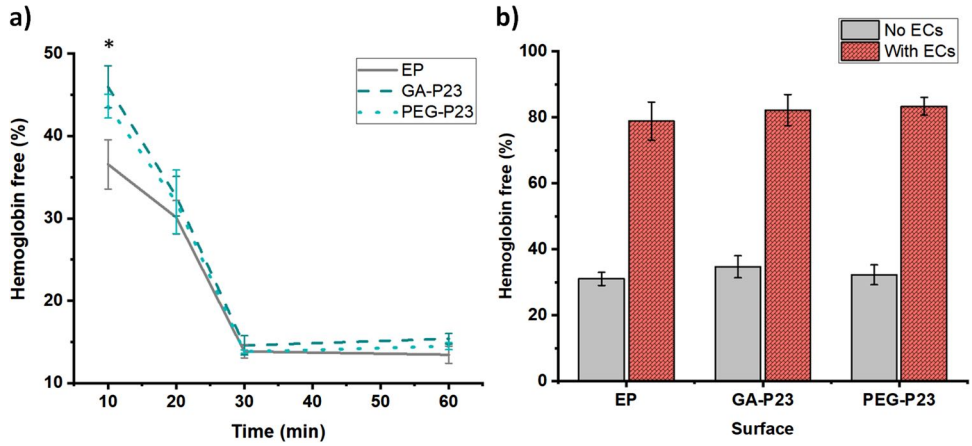

FIG. 5. Hemoglobin-free assays: (a) kinetics of coagulation for the different surfaces, it can be observed that after 10 min, there is a significant increase in the hemocompatibility on GA-P23 and PEG-P23 when compared to the bare metallic surface ($p < 0.01$).

C. Conformation of the peptide

After the biological performance and the composition of the surface, the distribution and the conformation of the peptide by ToF-SIMS, both in imaging and in static modes, respectively, were assessed. Regarding imaging mode, as observed in Fig. 6, three main fragments were studied: $C_4H_8N^+$ from proline, $C_2H_5O^+$ from the GA and PEG chains, and $Cr_2O_2^+$ from the oxide layer. Furthermore, for the imaging mode, the sum of all the specific fragments related to the amino acids was selected as well. It was found that the fragment related to proline was more present in the GA-P23 surface compared to PEG-P23, with a total count (TC) of 5.998×10^5 to 4.876×10^5, respectively. The other fragments related to the presence of the linking arm and the oxide layer were higher on PEG-P23, with a TC of 2.011×10^5 and 1.309×10^5 compared to 1.122×10^5 and 9.926×10^4 on GA-P23. Both surfaces, GA-P23 and PEG-23, presented a homogeneous peptide distribution on the surface, as observed by the sum of all the specific fragments related to the composition of the peptide. However, GA-P23 presented a higher intensity of peptide fragments, with a TC of 2.204×10^6 to 1.779×10^6 when compared to PEG-P23.

A comparison of the relative intensities (normalized to total counts) of the amino acids from the P23 grafted on the surface was performed in order to study the conformation of the peptide. As seen in Fig. 7, an increase in the fragments

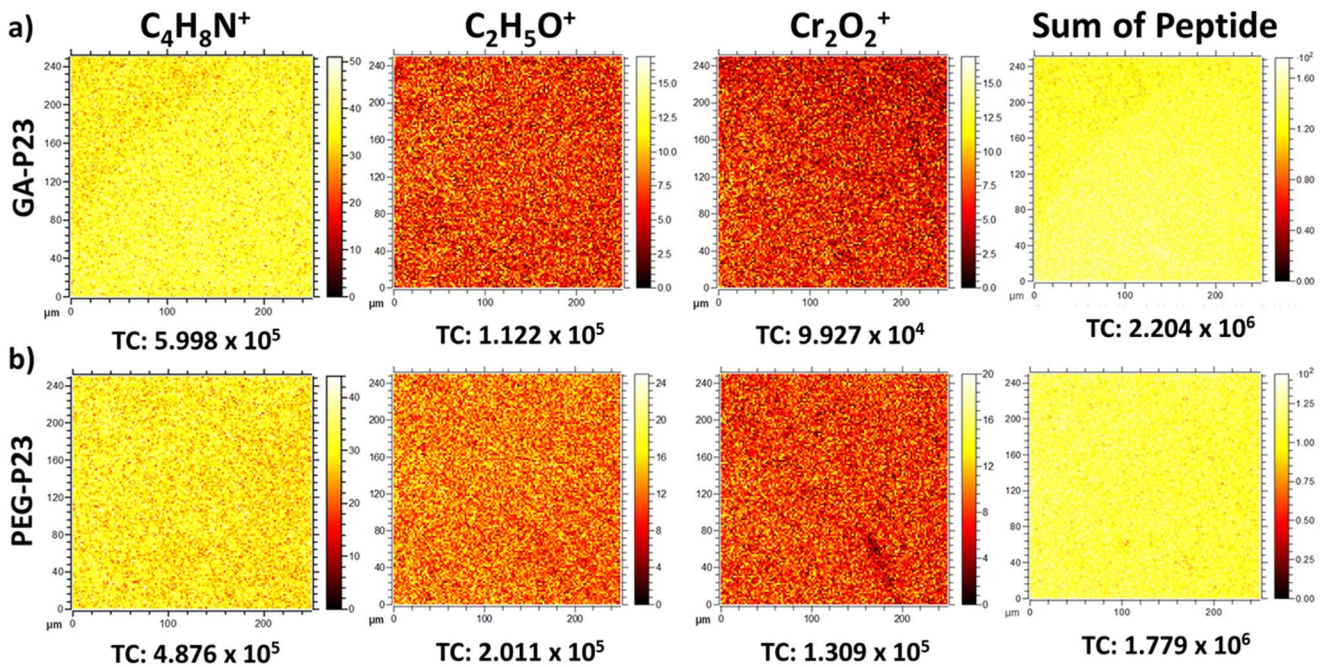

FIG. 6. ToF-SIMS images $250 \times 250\,\mu m^2$ of fragment $C_4H_8N^+$, proline (m/z 70.069), $C_2H_5O^+$ (m/z 45.032), as a characteristic fragment from the linking arm, $Cr_2O_2^+$ (m/z 135.871), as a fragment related to the oxide layer of the alloy and the sum of all the fragments related to the peptide composition: (a) GA-P23 sample and (b) PEG-P23. Both surfaces exhibited a homogeneous distribution of the peptide on the surface.

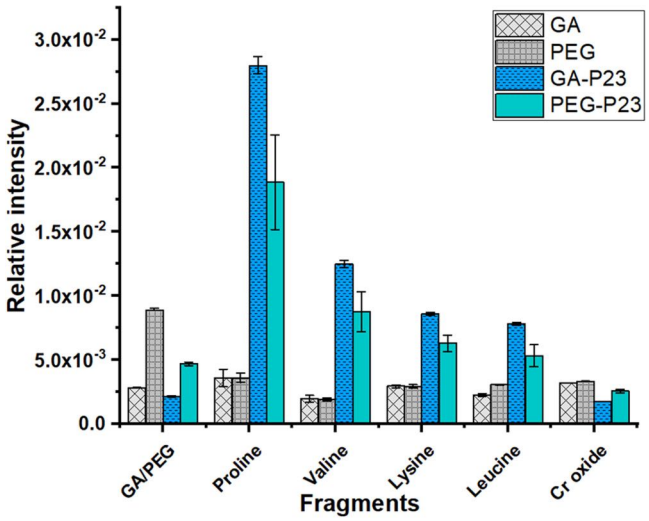

FIG. 7. ToF-SIMS analyses in positive static mode, a comparison of the relative intensities of the specific fragments of the amino acids that compound the peptide to confirm its presence on the surface due to a significant increase on the peptide fragment after grafting.

related to the peptide composition was found. Furthermore, in the same figure, the amino acid with the highest intensity for both GA-P23 and PEG-P23 surfaces was proline. Figure 7 shows that there are consistently less amino-acid fragments on PEG-P23 compared to GA-P23, implying a lower P23 grafting density when using PEG as a linking arm. This observation was in line with the XPS data, showing higher C and N concentrations on the GA-P23 surface. However, subtle differences were observed in the fragment's intensity drop from GA-P23 to PEG-P23, which can be related to conformation differences. In particular, the proline fragment intensity drop is more pronounced than for the other amino acids (valine, lysine, and leucine). The proline to lysine ratio is 3.27 ± 0.04 on GA-P23 and 2.99 ± 0.01 on PEG-P23, which is a small but significant difference indicating different conformations.

D. Transfer to cardiovascular devices

The feasibility of commercial stents functionalization with bioactive molecules was studied by grafting a modified version of the peptide with iodine in its composition. ToF-SIMS images of the surface in the positive and the negative ion modes were performed to study specific fragments related to the oxide layer and the peptide. As observed in Fig. 8, for positive ion mode, the fragment related to the oxide layer is Cr^+ while for the peptide, $C_4H_8N^+$, from proline, was selected. Regarding negative ion mode, the selected fragments for the oxide layer and the peptide were CrO_2^- and I^-, respectively. It was found that the fragments related to the peptide composition were present on the surface for both positive and negative modes. Furthermore, the metallic compounds were also present, confirming a functionalization but not a coating.

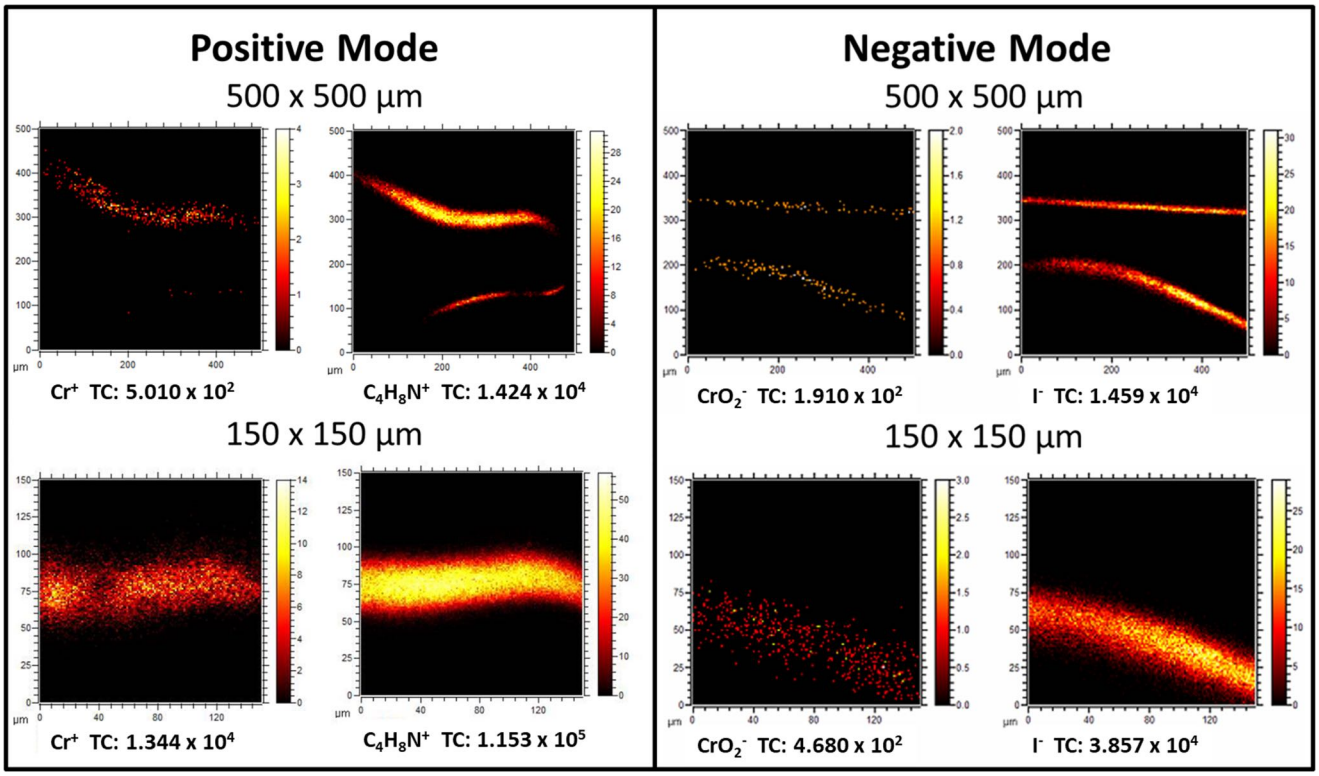

FIG. 8. ToF-SIMS images $500 \times 500\,\mu m^2$ and $150 \times 150\,\mu m^2$ of a commercial stent modified by this plasma-based strategy. Positive mode: fragment $C_4H_8N^+$, proline (m/z 70.071) from the peptide and Cr^+, as a fragment related to the metallic surface of the alloy (m/z 51.939). Negative mode: fragment I^-, iodine (m/z 126.904) from the peptide and CrO_2^- (m/z 83.932), as a fragment related to the metallic surface of the alloy.

IV. DISCUSSION

A. Surface characterization

From Table II, when comparing the surface chemical compositions after LA grafting, from the reference (the sample after plasma amination), a decrease of the percentage of nitrogen and metals can be observed. Furthermore, when grafting any of the linking arms, an increase in the percentage of carbon related to the chemical composition of both GA and PEG is observed. As the grafting procedure continues, with the addition of the P23 peptide, the percentage of nitrogen and carbon increases, while the percentage related to the oxide layer continues to decrease. These observations prove that the plasma-based strategy, shown in Fig. 1, allows the direct functionalization with bioactive molecules, but it does not create a fully covering coating as the metallic percentage remains large, as seen on XPS analyses. Moreover, the changes of the %C, %O, and %N for both GA-P23 and PEG-P23 were similar to what was expected from the theoretical peptide composition (%C = 64.7, %O = 15.8, and %N = 19.6). As regards GA to GA-P23, there was a large increase in %C of ∼8% and in %N of ∼2%, which was expected from the addition of the peptide. Nevertheless, the percentage of oxygen decreased by ∼5%, which is related to the partial coverage of the metallic surface by the grafted peptide with a short linking arm (five atoms of carbon) leading to a decrease of oxygen from the oxide layer. A similar trend was observed on PEG-P23; nevertheless, the increases were smaller when compared to GA-P23. As regards %C, only an increase of ∼2% was observed, while the %N increased only ∼1%. The N increase is due to the presence of the peptide at the surface. It was about twice less than in the GA case, which probably means that fewer peptide molecules were grafted. This was also confirmed by the lower intensity of amino acids' fragments in ToF-SIMS (Fig. 7). As for carbon, the relatively small increase was due to the small contribution of the peptide (119 atoms of carbon), which represents only a weak contribution compared to the long chain of PEG (Mn = 600, ∼1200 atoms of carbon). This effect was quite different when the peptide was grafted on the small GA linking arm, where carbon added by the peptide now represented a major contribution. Moreover, the changes in the chemical composition results were coherent from the point of view of the molecular length of the LA and the P23 peptide. The contribution of the P23 peptide, whose length is around 10.9 nm (C–C × 28 and C–N × 46), when grafted by GA with a 0.9 nm length (C–C × 5 and C–O × 1) is significantly much higher than when it is grafted by PEG. In this case, the length of the LA is around 170 nm ($[C–C \times 1 \text{ and } C–O \times 1]_{600}$) if considered in a linear conformation, thus, having more contribution than the 10.9 nm from the peptide.

The distribution of the grafted molecules on the first layer of the surface was assessed by the ToF-SIMS imaging mode, shown in Fig. 6. It was found that both linking arms presented a homogeneous distribution on the fragments related to the peptide. Nevertheless, GA-P23, Fig. 6(a), presented higher intensities for fragments related to proline and for the sum of the peptide fragments, which suggested that the bioactive molecule was more exposed to the surface when compared to PEG-P23 [Fig. 6(b)]. The signal from the metal oxide ($Cr_2O_2^+$) was higher on PEG-P23 compared to GA-P23. Again, this suggested that less peptide was grafted in PEG-P23, so that the metallic substrate was less covered, giving rise to a higher secondary ion signal from the oxide compared to GA-P23.

B. Biological performance

After studying the chemical composition of both GA-P23 and PEG-P23 and the physical distribution of the biomolecule on the flat samples, biological tests were performed to evaluate the toxicity of the surface, endothelialization, and hemocompatibility. Regarding the toxicity of the surface, a cell viability test with endothelial cells was performed (Fig. 3). It was found that, since day 1, GA-P23 and PEG-P23 presented significantly higher cell viability compared to the bare metal surface (electropolished control); this higher cell viability continued up to 7 days where only PEG-P23 continued to be significantly different. These results were completed with a migration assay to simulate the wound healing after the implantation of the cardiovascular device where a fast formation of a monolayer of endothelial cells is desired.[33] Results for this migration test, Fig. 4, were according to what was previously found in the cell viability assay: PEG-P23 was the surface that presented a faster migration of endothelial cells, which can be clearly observed after 3 days of migration. Furthermore, after 7 days of migration, PEG-P23 presented a complete monolayer of endothelial cells on the surface, confirmed by showing the highest intensity on the staining related to the intercellular junctions (VE-cadherin).[34] This behavior could be related to two properties related to PEG as linking arm: (a) The potential synergic effect of the antifouling properties of PEG, and the bioactivity of the peptide. Even if a PEG of Mn = 600 is considered a small chain PEG, it had already been previously confirmed that can present this antifouling behavior when grafted onto a surface.[35] This synergic effect could have promoted the specific interaction between the endothelial cells and the peptide, leading to their faster migration. (b) Due to a higher degree of freedom conferred by the long chain of PEG the peptide can expose its active site to the cells faster than GA, which could be restricted by its small chain. Similar observations have already been found for other proteins when grafted by PEG.[36]

Hemocompatibility was studied due to the potential properties of the peptide and for its importance to decrease complications after stent implantation. It was found that the presence of the peptide significantly increased blood compatibility during the first minutes of contact (10 min) for both GA-P23 and PEG-P23 when compared to the bare metallic surface, as shown in Fig. 5(a). However, no difference was found between the linking arms. Following the blood coagulation kinetics, it was found that after this time, no significant

difference was found among the surfaces and after 30 min, a clot was completely formed. Furthermore, blood compatibility studies were also performed on endothelialized surfaces, Fig. 5(b), where it was found that the presence of ECs on the surface prevented clot formation at 20 min. No significant difference was observed between any surfaces since ECs can attach and also proliferate on the bare metallic surface, as previously confirmed on the cell viability studies (Fig. 3).

These findings suggested that the mechanism of action of the P23 peptide to enhance the biocompatibility of the L605 metallic surface is first to promote a fast endothelialization by a signal/receptor interaction between the surface with the immobilized PECAM-1 peptide and the endothelial cells which lead to an increase in the blood compatibility caused by the attachment and coverage of the metallic surface by endothelial cells.

C. Conformation of the peptide

To further understand why the biological performance on both surfaces was similar and how the peptide was arranged on the surface, the conformation of the immobilized bioactive molecule was studied using ToF-SIMS in a static positive mode. Relative intensities, shown in Fig. 7, indicated that the most intense fragment for both GA-P23 and PEG-P23 was from proline, $C_4H_8N^+$, which as observed in Fig. 9(a), is present twice in the composition of the peptide. Proline fragments, as well as the other fragments from the peptide, are always more intense on GA-P23 than on PEG-P23, again confirming a higher peptide surface density on GA-P23. However, the biological activity appears better on PEG-P23 even if less peptide is available. This could be due to a different conformation of the peptide. Indeed, when looking carefully at the intensity changes from GA-P23 to PEG-P23, the valine, lysine, and leucine relative drops are similar, while the proline drop is significantly stronger. The proline to valine ratio is 3.27 ± 0.04 on GA-P23, while it is 2.99 ± 0.01 on PEG-P23, a small but statistically relevant difference. If the peptide chains had random orientations for both LA, there should be no observable differences between the amino-acid fragments relative intensities. If a preferential conformation exists on one of the LAs, subtle variations of the relative intensities should be observed, as is the case in this study. The slightly higher proline intensity on GA-P23 suggests that the peptide conforms in such a way that proline is more exposed on the surface. On the other hand, the polymeric PEG chains, long compared to the short GA molecule, will tend to fold at the surface so that the grafted peptides will present random orientations. Taking under consideration these results and the fact that ToF-SIMS analyses are performed under high vacuum, Figs. 9(b) and 9(c) present the potential conformation for GA-P23 and PEG-P23, respectively. This conformation was proposed considering that, for this immobilization strategy, free amine groups are needed, as observed in the reaction schematics (Fig. 1), and based on the high intensity of proline on both linking arms, the most probable zone where the peptide is grafted is either by the arginine or by the middle lysine [located in the bottom of the 3D model shown Fig. 9(a)]. Thus, Fig. 9(b) shows a potential conformation for GA-P23 which under vacuum exposes the peptide and that once in contact with the cells, due to a low degree of freedom conferred by the small linking arm, the peptide could not expose the bioactive site so easily, leading to a slower biological response, especially in terms of endothelial cell migration, as seen in Fig. 4. On the other hand, PEG-P23, Fig. 9(c), under vacuum was in a folded state caused by the shrinking of the PEG chains, partially hiding the peptide. However, once this surface was in contact with the endothelial cells, due to the longer chain and higher degree of freedom, a faster biological response was obtained; thus, a faster cell migration that could lead to promote re-endothelialization and avoid thrombus formation on cardiovascular devices, as suggested by hemocompatibility studies (Fig. 5).

D. Transfer to cardiovascular devices

Finally, the feasibility to transfer this technology onto bare metal stents was assessed by ToF-SIMS imaging in both positive and negative modes. Similar studies had

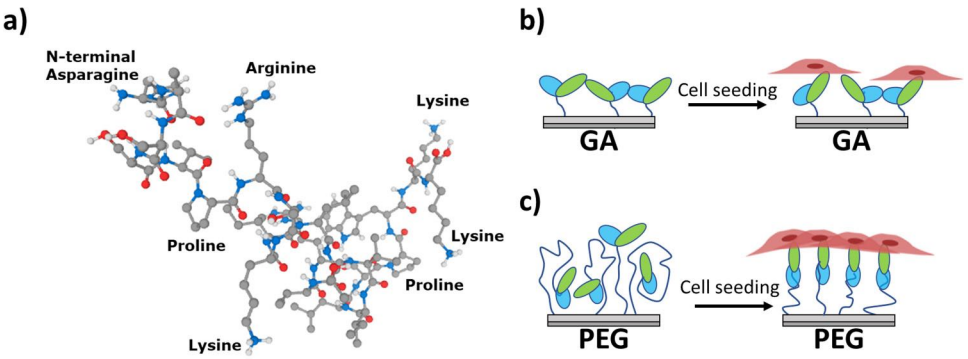

FIG. 9. Schematics of (a) P23 peptide 3D model, (b) proposed conformation of GA-P23 before (under vacuum) and after cell seeding, with a potential steric impediment that does not allow the peptide to expose the bioactive site for ECs, and (c) proposed conformation for PEG-P23, which under vacuum it shrinks and exposes the linking arm onto the surface hiding the peptide but when in contact with the cell medium it allows the bioactive peptide to obtain the optimal conformation which promotes cell adhesion.

already been performed on flat samples to confirm the immobilization of a peptide modified with iodine.[21] As shown in Fig. 8, fragments studied in the positive mode were Cr^+ from the metallic surface and proline from the immobilized peptide. In the negative ion mode, the fragment related to the metallic surface was CrO_2^- and I^- for the peptide. The presence of these fragments confirmed the direct immobilization of the peptide onto the metallic cardiovascular device. Moreover, the presence of the fragments related to the alloy confirmed a functionalization and not a coating. This confirmation opens a new alternative to what can be currently found in the market: bare metallic stents or drug-eluting stents, which use polymeric coatings to elute drugs.

V. CONCLUSIONS

It was possible to graft a CD31 derived peptide onto the surface of L605 cobalt chromium without the use of any polymeric matrix, by using a plasma-based multistep treatment. This technique allowed to graft the peptide by different linking arms, GA and PEG, confirmed by following the chemical composition changes of the surface by XPS and ToF-SIMS. It was found that both LA increased the biological performance of the surface, on endothelialization and hemocompatibility, when compared to the bare metallic one. However, PEG-P23 demonstrated the most promising properties to be used for the stent application due to its fast endothelialization that could lead to antithrombotic activity. The advantage of PEG over GA is its long and mobile chain, allowing the peptide to better reach out to the endothelial cells. Furthermore, by ToF-SIMS analyses, it was possible to confirm the grafting of a peptide onto the surface of a commercial stent, proving that this novel procedure may be used not only on flat structures but also onto complex 3D structures. By using this technique combined with newly developed drugs that can promote the biological properties desired for the stent application, a new generation of commercial devices can be developed.

ACKNOWLEDGMENTS

Sergio Diaz-Rodriguez is a recipient of a Ph.D. scholarship from the NCPRM (www.ncprm.ulaval.ca). This work was supported by the Natural Sciences and Engineering Research Council of Canada (NSERC), the CHU de Québec Research Center, The Ministry of Economy, Science and Innovation of Quebec, and the Linkage Grants Québec/Wallonie-Brussels of the Ministry of International Relations and "La francophonie" of Quebec.

[1]G. Mani, M. D. Feldman, D. Patel, and C. M. Agrawal, Biomaterials **28**, 1689 (2007).
[2]R. A. Lange, J. E. Willard, and L. D. Hillis, Am. J. Med. Sci. **306**, 265 (1993).
[3]D. R. Holmes, R. S. Schwartz, and M. W. I. Webster, J. Am. Coll. Cardiol. **17**, 14 (1991).
[4]G. Dangas and V. Fuster, Am. Heart J. **132**, 428 (1996).
[5]J. F. Granada, G. L. Kaluza, and A. Raizner, Curr. Atheroscler. Rep. **5**, 308 (2003).
[6]H. Takahashi, D. Letourneur, and D. W. Grainger, Biomacromolecules **8**, 3281 (2007).
[7]M. Takano *et al.*, Circ. Cardiovasc. Interv. **3**, 476 (2010).
[8]R. A. Byrne, R. Iijima, J. Mehilli, S. Pinieck, O. Bruskina, A. Schömig, and A. Kastrati, JACC Cardiovasc. Interv. **2**, 291 (2009).
[9]A. Kastrati and R. Byrne, JACC Cardiovasc. Interv. **4**, 165 (2011).
[10]K. Vallières, É. Petitclerc, and G. Laroche, Macromol. Biosci. **7**, 738 (2007).
[11]H. C. Lowe, S. N. Oesterle, and L. M. Khachigian, J. Am. Coll. Cardiol. **39**, 183 (2002).
[12]J. M. Kim *et al.*, Prog. Org. Coat. **78**, 348 (2015).
[13]V. Montaño-Machado *et al.*, "Medical devices: Coronary stents," in *Reference Module in Biomedical Sciences* (Elsevier, 2017), pp 386–398.
[14]G. Caligiuri and A. Nicoletti, WIPO, No. Wo 2010/000741 a1 (7 January 2010)
[15]Z. Ming, Y. Hu, J. Xiang, P. Polewski, P. J. Newman, and D. K. Newman, Blood **117**, 3903 (2011).
[16]G. Cao, C. D. O'Brien, Z. Zhou, S. M. Sanders, J. N. Greenbaum, A. Makrigiannakis, and H. M. DeLisser, Am. J. Physiol. Cell Physiol. **282**, C1181 (2002).
[17]P. Roach, D. Eglin, K. Rohde, and C. C. Perry, J. Mater. Sci. Mater. Med. **18**, 1263 (2007).
[18]G. Sydow-Plum and M. Tabrizian, Mater. Sci. Technol. **24**, 1127 (2008).
[19]M. Cloutier, S. Turgeon, P. Chevallier, and D. Mantovani, Adv. Mater. Res. **409**, 117 (2011).
[20]B. Akhavan *et al.*, Appl. Mater. Today **16**, 456 (2019).
[21]S. Diaz-Rodriguez, P. Chevallier, and D. Mantovani, Plasma Process. Polym. **15**, 1700214 (2018).
[22]A. A. John, A. P. Subramanian, M. V. Vellayappan, A. Balaji, S. K. Jaganathan, H. Mohandas, T. Paramalinggam, E. Supriyanto, and M. Yusof, RSC Adv. **5**, 39232 (2015).
[23]G. Honari, S. G. Ellis, B. L. Wilkoff, M. A. Aronica, L. G. Svensson, and J. S. Taylor, Contact Dermatitis **59**, 7 (2008).
[24]Y. Hu, S. R. Winn, I. Krajbich, and J. O. Hollinger, J. Biomed. Mater. Res. **64A**, 583 (2003).
[25]V. Montaño-Machado, L. Hugoni, S. Díaz-Rodríguez, R. Tolouei, E. Pauthe, and D. Mantovani, Phys. Chem. Chem. Phys. **18**, 1 (2016).
[26]C. Holmes and M. Tabrizian, *Stem Cell Biology and Tissue Engineering in Dental Sciences* (Elsevier, 2015), pp. 187–206.
[27]C. S. Campelo, P. Chevallier, J. M. Vaz, R. S. Vieira, and D. Mantovani, Mater. Sci. Eng. C **72**, 682 (2017).
[28]J. M. Vaz, T. B. Taketa, J. Hernandez-Montelongo, P. Chevallier, M. A. Cotta, D. Mantovani, and M. M. Beppu, Appl. Surf. Sci. **445**, 478 (2018).
[29]C. Loy, S. Meghezi, L. Lévesque, D. Pezzoli, H. Kumra, D. Reinhardt, J. N. Kizhakkedathu, and D. Mantovani, Biomater. Sci. **5**, 153 (2017).
[30]M. Henry and P. Bertrand, Surf. Interface Anal. **41**, 105 (2009).
[31]J.-B. Lhoest, M. S. Wagner, C. D. Tidwell, and D. G. Castner, J. Biomed. Mater. Res. **57**, 432 (2001).
[32]S. Diaz-Rodriguez, P. Chevallier, C. Paternoster, V. Montaño-Machado, C. Noël, L. Houssiau, and D. Mantovani, RSC Adv. **9**, 2292 (2019).
[33]F. Copes *et al.*, Potential. Adv. Med. Sci. **64**, 144 (2019).
[34]E. Dejana, M. Corada, and M. G. Lampugnani, FASEB J. **9**, 910 (1995).
[35]B. Dong, H. Jiang, S. Manolache, A. C. L. Wong, and F. S. Denes, Langmuir **23**, 7306 (2007).
[36]E. C. Michel, V. Montaño-Machado, P. Chevallier, A. Labbé-Barrère, D. Letourneur, and D. Mantovani, Biomatter **4**, F28805 (2014).